KLOE Memo 214
June 30, 2000

First Results from $\phi \to K_L K_S$ Decays with the KLOE Detector

The KLOE collaboration

Abstract

The KLOE experiment has collected 2.4 pb^{-1} of integrated luminosity during the commissioning of the DAΦNE ϕ-factory in 1999. The performance of the detector has been studied using the $\phi \to K_L K_S$ decays collected during this period, yielding also first measurements of relevant K parameters such as masses and lifetimes. A clean $K_S \to \pi^+\pi^-$ sample is used to select $K_L \to \pi^+\pi^-$ CP-violating decays and $K_L \to K_S$ regeneration events in the detector material. Results on the regeneration probability in a beryllium-alluminum alloy and carbon-fiber plus aluminum composite are presented.

Contributed paper ♯ 294 to the XXX International Conference on High Energy Physics, Osaka 27 jul - 2 aug 2000.

M. Adinolfi,[m] A. Aloisio,[g] F. Ambrosino,[g] A. Andryakov,[f] A. Antonelli,[c] M. Antonelli,[c] F. Anulli,[c] C. Bacci,[n] A. Bankamp,[d] G. Barbiellini,[q] F. Bellini,[n] G. Bencivenni,[c] S. Bertolucci,[c] C. Bini,[k] C. Bloise,[c] V. Bocci,[k] F. Bossi,[c] P. Branchini,[n] S. A. Bulychjov,[f] G. Cabibbo,[k] A. Calcaterra,[c] R. Caloi,[k] P. Campana,[c] G. Capon,[c] G. Carboni,[m] A. Cardini,[k] M. Casarsa,[q] G. Cataldi,[d] F. Ceradini,[n] F. Cervelli,[j] F. Cevenini,[g] G. Chiefari,[g] P. Ciambrone,[c] S. Conetti,[r] E. De Lucia,[k] G. De Robertis,[a] R. De Sangro,[c] P. De Simone,[c] G. De Zorzi,[k] S. Dell'Agnello,[c] A. Denig,[d] A. Di Domenico,[k] C. Di Donato,[g] S. Di Falco,[j] A. Doria,[g] E. Drago,[g] V. Elia,[e] O. Erriquez,[a] A. Farilla,[n] G. Felici,[c] A. Ferrari,[n] M. L. Ferrer,[c] G. Finocchiaro,[c] C. Forti,[c] A. Franceschi,[c] P. Franzini,[k,i] M. L. Gao,[b] C. Gatti,[c] P. Gauzzi,[k] S. Giovannella,[c] V. Golovatyuk,[e] E. Gorini,[e] F. Grancagnolo,[e] W. Grandegger,[c] E. Graziani,[n] P. Guarnaccia,[a] U. v. Hagel,[d] H. G. Han,[b] S. W. Han,[b] X. Huang,[b] M. Incagli,[j] L. Ingrosso,[c] Y. Y. Jiang,[b] W. Kim,[o] W. Kluge,[d] V. Kulikov,[f] F. Lacava,[k] G. Lanfranchi,[c] J. Lee-Franzini,[c,o] T. Lomtadze,[j] C. Luisi,[k] C. S. Mao,[b] M. Martemianov,[f] A. Martini,[c] M. Matsyuk,[f] W. Mei,[c] L. Merola,[g] R. Messi,[m] S. Miscetti,[c] A. Moalem,[h] S. Moccia,[c] M. Moulson,[c] S. Mueller,[d] F. Murtas,[c] M. Napolitano,[g] A. Nedosekin,[c,f] M. Panareo,[e] L. Pacciani,[m] P. Pagès,[c] M. Palutan,[m] L. Paoluzi,[m] E. Pasqualucci,[k] L. Passalacqua,[c] M. Passaseo,[k] A. Passeri,[n] V. Patera,[l,c] E. Petrolo,[k] G. Petrucci,[c] D. Picca,[k] G. Pirozzi,[g] C. Pistillo,[g] M. Pollack,[o] L. Pontecorvo,[k] M. Primavera,[e] F. Ruggieri,[a] P. Santangelo,[c] E. Santovetti,[m] G. Saracino,[g] R. D. Schamberger,[o] C. Schwick,[j] B. Sciascia,[k] A. Sciubba,[l,c] F. Scuri,[q] I. Sfiligoi,[c] J. Shan,[c] P. Silano,[k] T. Spadaro,[k] S. Spagnolo,[e] E. Spiriti,[n] C. Stanescu,[n] G. L. Tong,[b] L. Tortora,[n] E. Valente,[k] P. Valente,[c] B. Valeriani,[j] G. Venanzoni,[d] S. Veneziano,[k] Y. Wu,[b] Y. G. Xie,[b] P. P. Zhao,[b] Y. Zhou[c]

[a] Dipartimento di Fisica dell'Università e Sezione INFN, Bari, Italy.
[b] Institute of High Energy Physics of Academica Sinica, Beijing, China.
[c] Laboratori Nazionali di Frascati dell'INFN, Frascati, Italy.
[d] Institut für Experimentelle Kernphysik, Universität Karlsruhe, Germany.
[e] Dipartimento di Fisica dell'Università e Sezione INFN, Lecce, Italy.
[f] Institute for Theoretical and Experimental Physics, Moscow, Russia.
[g] Dipartimento di Scienze Fisiche dell'Università e Sezione INFN, Napoli, Italy.
[h] Physics Department, Ben-Gurion University of the Negev, Israel.
[i] Physics Department, Columbia University, New York, USA.
[j] Dipartimento di Fisica dell'Università e Sezione INFN, Pisa, Italy.
[k] Dipartimento di Fisica dell'Università e Sezione INFN, Roma I, Italy.
[l] Dipartimento di Energetica dell'Università, Roma I, Italy.
[m] Dipartimento di Fisica dell'Università e Sezione INFN, Roma II, Italy.
[n] Dipartimento di Fisica dell'Università e Sezione INFN, Roma III, Italy.
[o] Physics Department, State University of New York at Stony Brook, USA.
[q] Dipartimento di Fisica dell'Università e Sezione INFN, Trieste/Udine, Italy.
[r] Physics Department, University of Virginia, USA.
* Associate member

1 Introduction

The DAΦNE ϕ factory [1] has come into operation in july 1999, delivering 2.4 pb^{-1} of integrated luminosity to the KLOE experiment during its commissioning period. Such data allowed to perform a careful check of the detector operation and performances [2].

A sample of $\phi \to K_S K_L$ decays provided a source of monochromatic, 110 MeV/c ($\beta = 0.21$), beams of K_S and K_L mesons, which were reconstructed in various decay modes.

A preliminary measurement of the K_S lifetime was performed in a subsample of events. Charged decays oh the K_L were also reconstructed, and a sample of CP violating $K_L \to \pi^+\pi^-$ decays was selected. The probability of $K_L \to K_S$ regeneration in the materials of the KLOE detector was also measured. With the available statistics it was possible to clearly identify regeneration events produced in the beam-pipe, made of a Beryllium-Aluminum alloy, and in the drift chamber wall, made of Carbon fiber, and to measure the angular dependence of the cross section.

2 Experimental setup

The KLOE experiment [2] consists of a large volume tracking detector surrounded by a hermetic calorimeter both immersed in the axial magnetic field of 0.56 T produced by a superconducting coil. The tracking detector is a cylindrical drift chamber with alternated stereo views. The sensitive volume, 25 cm inner radius, 195 cm outer radius and 320 cm length is filled with a 90%Helium-10%Isobutane gas mixture. Charged particle tracks are reconstructed in 12582 drift cells arranged in 58 concentric layers. The spatial resolution in the transverse plane is about 150 μm.

The calorimeter, made with 1 mm diameter scintillating fibers immersed in 0.5 mm grooved lead plates, has a thickness of 23 cm corresponding to 15 X_0. It is segmented in 288 sectors in the barrel and 200 in the endcaps, each sector being subdivided in five longitudinal samplings. Energy clusters are reconstructed with a resolution $\sigma_E/E = 0.057/[E\ (GeV)]^{1/2} \oplus 0.006$ and a space resolution of few cm. Time of flight measurement with a resolution of $\sigma_t = 0.05\ ns/[E\ (GeV)]^{1/2} \oplus 0.14\ ns$ is used for particle identification.

Data were taken at the energy of the ϕ resonance for six weeks in the period august-december 1999 during the commissiong of the DAΦNE collider. Typical values of the beam parameters are listed in Table 1. The beams cross with a period multiple of 2.7 ns and with an angle of 25 mrad in the horizontal plane. This implies a small boost of 13 MeV of the center of mass relative to the experiment.

numer of bunches	20 e^+ + 20 e^-
beam currents	300 mA
beam luminosity	$10^{30}\ cm^{-2}s^{-1}$
luminosity lifetime	$\approx$ 30 min

Table 1: Typical values of the DAΦNE beam parameters during data dating.

The trigger requirement during most of the data taking was at least two calorimeter energy deposits in the configurations Barrel-Barrel or Barrel-EndCap with E(Barrel)>

50 MeV and E(Endcap)> 90 MeV. This trigger has an average efficiency [9] of about 90% for most of the ϕ decays and of about 84% for $\phi \to K_L K_S$ events with K_L and K_S decaying into charged particles of interest for this analysis. The trigger rate was typically 1.5 kHz mostly due to cosmic rays. The luminosity was measured with an accuracy of about 5% by recording Bhabha scattering events in the polar angle interval $22^o < \theta < 158^o$.

2.1 Data sample

About 8 million ϕ decays were collected during data taking. The data were filtered against cosmics and machine background, and then classified in 5 different classes [3]:

1. $\phi \to K_S K_L$
2. $\phi \to K^+ K^-$
3. ϕ radiative decays
4. $\rho\pi$ events
5. Bhabhas

This analysis used only events in class 1 where a candidate K_S charged decay was present, satisfying the following requirements: one vertex made with two tracks of opposite curvature with $\rho = (x^2 + y^2)^{1/2} < 4$ cm, $|z| < 8$ cm, two pion invariant mass $400 < m < 600$ MeV, and total momentum $50 < p < 120$ MeV.

3 Measurement of the K_S lifetime

3.1 Measurement Technique

The position of the secondary vertex (SV) of $\pi^+\pi^-$ pairs from K_s decays, together with the knowledge of the position of e^+e^- primary vertex (PV, the luminous region) allows the measurement of the K_s decay length in the ϕ frame, $\lambda_s = \beta\gamma c\tau_s$. X_{PV} and Y_{PV} are reconstructed run-by-run from Bhabha scattering events with a typical accuracy of few tens of microns and have widths L(X), L(Y) which are small compared to the 6 mm K_s decay length [4], [5]. L(X) = 1.0 mm is measured by KLOE and L(Y) = few tens of microns is measured by DAΦNE. Z_{PV} is also reconstructed run-by-run with 100-200 μm accuracy, but it has a width of 12-14 mm, which distorts the K_s lifetime distributions. Therefore, Z_{PV} is computed event by event using the polar angle (θ_s) of the K_s momentum (p_s) :

$$Z_{PV} = Z_{SV} + cot(\theta_s) \times \sqrt{(X_{PV} - X_{SV})^2 + (Y_{PV} - Y_{SV})^2}. \quad (1)$$

The effectiveness of this procedure is demonstrated by extrapolating the K_s trajectory from the SV to the PV along $\vec{p_s}/p_s$. Fig.1 shows the difference between the intercept and the PV coordinate for x, y, and z, respectively (the selection of the data sample in these plots is described in the following section).

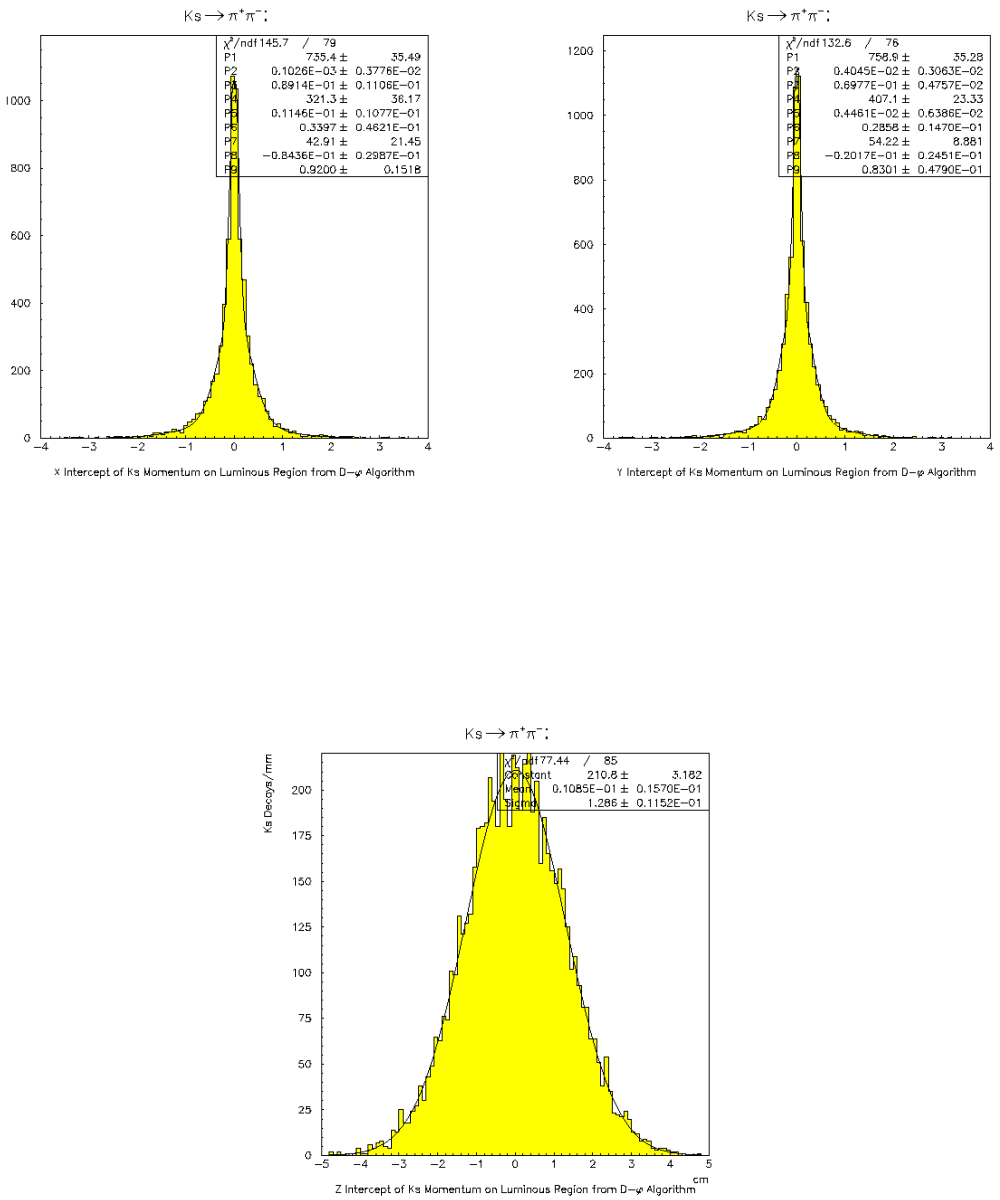

Figure 1: Projections of $\vec{p}_s$ distance of closest approach to the PV

To avoid the systematic distortion of the lifetime distribution due to the SV resolution (which from Figs.1 is shown to be comparable to the K_s lifetime itself), the following estimator is used:

$$\lambda = (\vec{r}_{SV} - \vec{r}_{PV}) \cdot \frac{\vec{p_s}}{p_s}. \tag{2}$$

λ is the K_s decay length projected on the $\vec{p_s}$ direction. λ_s can then be extracted from the fit to the λ distribution using an exponential appropriately smeared with PV and SV resolution functions. Since from direct measurement L(X) = 1.0 mm and from Monte Carlo studies $\sigma(\theta_s), \sigma(\phi_s) \sim$ few tens of mrad, the resolution on the plots of Fig.1 can be interpreted in terms of the SV resolution, that turns out to be by far the dominant contribution.

Finally, λ is Lorentz-transformed to the ϕ system using the run-average ϕ boost as measured from Bhabha events [5].

3.2 Sample Selection

This analysis was performed using only a subsample of events for which the position of the luminous region had been computed after data taking. The selection required the simultaneous presence of the K_S candidate vertex and of a second two-track vertex outside a sphere of 11 cm radius. If there is a third vertex the event is rejected. The following cuts are then imposed to the K_s candidates inside the beam pipe:

(1) 493 MeV $< M_s <$ 497 MeV,

(2) in the ϕ-CMS frame, 105 MeV $< P_s <$ 114 MeV,

(3) in the ϕ-CMS frame, $45° < \theta_s < 135°$,

(4) $|cot\theta(\pi, LAB)| < 1.0$ for both pions.

The final selected sample is 6866 decays.

3.3 Results

The lifetime distribution for the 6866 decays was fit to four different functions, with the constraint of the total number of decays:

(1) fit to an exponential smeared with two gaussian resolutions.

(2) fit to an exponential smeared with three gaussian resolutions.

(3) fit to an exponential smeared with two gaussian resolutions plus a third gaussian modeling a zero-lifetime component (due to background and/or to any other systematic effect).

(4) fit to an exponential smeared with three gaussian resolutions plus a fourth gaussian modeling a zero-lifetime component (due to background and/or to any other systematic effect).

As an exanple cases (2) and (4) are shown in fig.2. In both fits the parameter P1 is λ_s and P2 and P3 (P4 and P5) are the populations and standard deviation of the first (second) smearing gaussian. In case (2) P6 is the standard deviation of the third smearing gaussian, while in case (4) P6 and P7 are the population and standard deviation of the third smearing gaussian and P8 is the standard deviation of the fourth non-smearing gaussian. The results of the four fits are reported in table 2.

fit function	λ_s (mm)
2g smearing	5.71 $\pm$ 0.06
3g smearing	5.71 $\pm$ 0.06
2g smearing + 1g non smearing	5.90 $\pm$ 0.08
3g smearing + 1g non smearing	5.83 $\pm$ 0.07

Table 2: Typical values of the DAΦNE beam parameters during data dating.

The average λ_s value from the four fits is 5.78 mm. The fit statistical error on λ_s is taken as the largest fit error, 0.08 mm, while the fit systematic error is taken as half the difference between the maximum and minimum values of λ_s, 0.10 mm. The preliminary result is then:

$$\lambda_s \;=\; 5.78 \;\pm\; 0.08\,(stat) \;\pm\; 0.10\,(syst)\,mm$$

4 Measurement of the $K_L \to K_S$ regeneration cross section

Due to the different absorbtion cross section of K^o and $\bar{K}^o$, a pure beam of K_L mesons will regenerate [6] K_S mesons when traversing the detector. Thus $K_L \to K_S \to \pi\pi$ is a potential source of background for the rare $K_L \to \pi\pi$ CP-violating decays in experiments where high precision in event counting is required.

Regeneration is well studied at high energy but there is lack of experimental results at energies below 500 MeV. On the other hand theoretical predictions on the $K_L \to K_S$ regeneration cross section at low energy suffer of large uncertainties. It has been shown [7] that for a thin regenerator, $t < \lambda_S$, the coherent regeneration is negligible. Inelastic regeneration can also be considered negligible in 110 MeV/c K_L-nuclei interactions. Theoretical calculations [8] on incoherent K_L regeneration, based on the eikonal approximation and the Woods-Saxon form for the nuclear potential, foresee values in the range of 20-50 mb for the regeneration cross section on nuclei.

4.1 Data analysis

$K_S \to \pi^+\pi^-$ candidates were selected as described in sect. 2.1. The additional requirement of the presence of at least one more vertex, with two unlike sign tracks, was made.

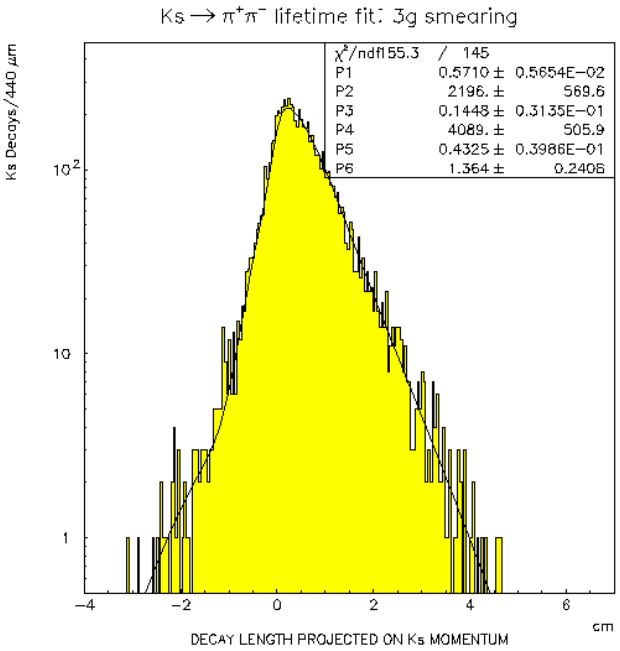

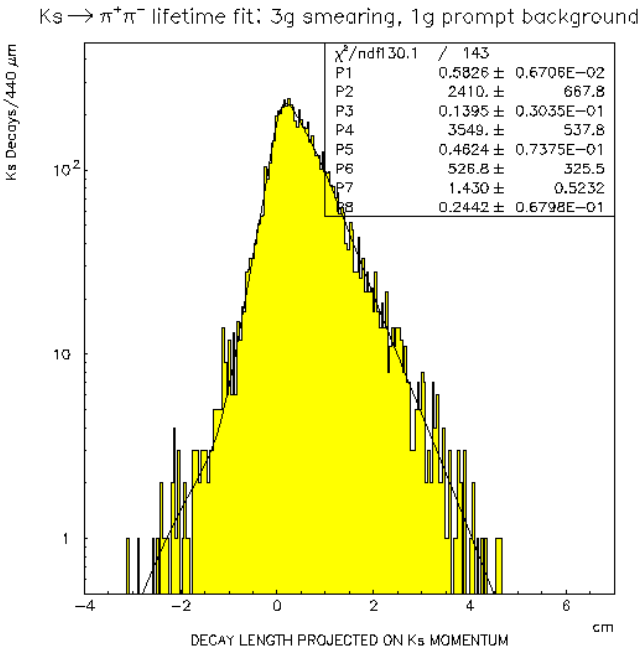

Figure 2: K_s decay length fit to an exponential smeared with three gaussians without and with a fourth non-smearing gaussian.

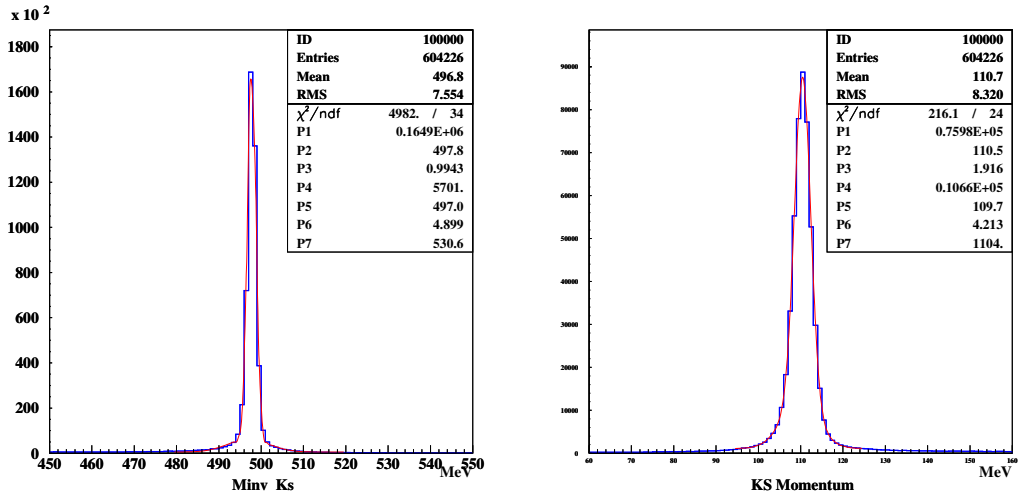

Figure 3: Distribution of the K_S vertex invariant mass and momentum

The distribution of the invariant mass and of the vector sum of the momenta in the ϕ-reference system are shown in Fig.3 for the selected 604226 vertices (592687 events). A clear peak at the K_S mass and at $p_S = 110$ MeV/c is observed. The off-peak values are mainly due to $\pi \to \mu\nu$ decays in flight and to reconstruction errors.

Fitting the distributions with two gaussians, the peak r.m.s. widths are $\sigma_m = 1.0$ and $\sigma_p = 1.9$ MeV. 445347 well reconstructed $K_S \to \pi^+\pi^-$ decays were selected requiring

$$\left(\frac{m - \langle m \rangle}{\sigma_m}\right)^2 + \left(\frac{p - \langle p \rangle}{\sigma_p}\right)^2 < 16$$

To search for the associated K_L decay vertex we first defined the K_L origin (the ϕ vertex) as the distance of closest approach between the K_S direction and the beam line (z axis). Events were retained requiring for the vertex position

$$\left(\frac{x - \langle x \rangle}{\sigma_x}\right)^2 + \left(\frac{y - \langle y \rangle}{\sigma_y}\right)^2 + \left(\frac{z - \langle z \rangle}{\sigma_z}\right)^2 < 9$$

where $\sigma_x = 0.63\,cm$, $\sigma_y = 0.59\,cm$ and $\sigma_z = 1.38\,cm$ are the r.m.s. widths of the ϕ vertex distributions. 433786 vertices (433760 events) satisfied this cut. When more than one vertex were found in the K_S fiducial volume, the vertex associated with the invariant mass closer to the peak value was retained. This is the $K_S K_L$ sample.

Associated charged decays of the K_L were then searched for. The K_L decay vertex is any second vertex reconstructed with two unlike sign tracks found in a cone opposite to the K_S direction in the ϕ reference system. Fig.4 shows the distribution of the angle δ between the direction of the K_L, defined by $-\vec{p}_S$, and the line joining the K_L vertex and the ϕ vertex, for different intervals of the distance d between the two vertices. From such distributions we derived the angle resolution, $\sigma_\delta = 18$ mrad,

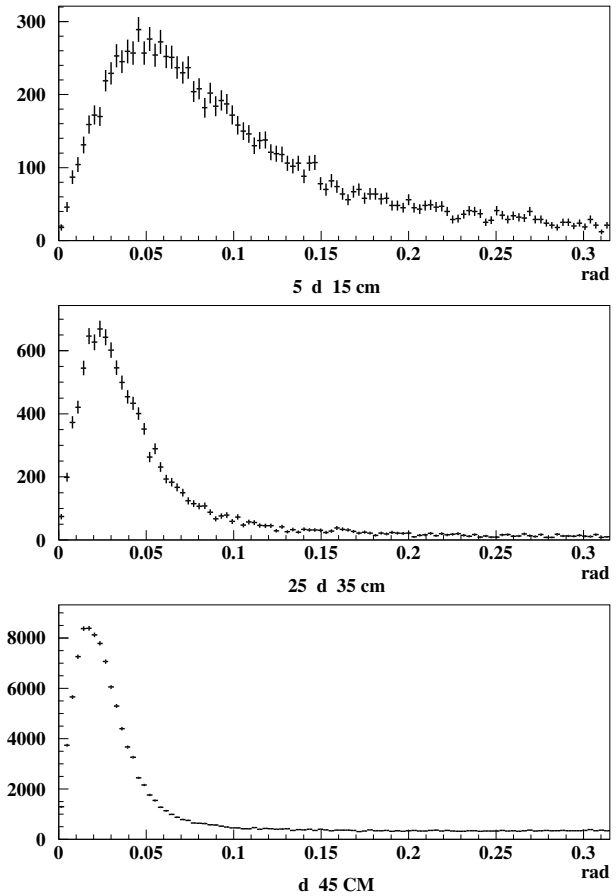

Figure 4: Distribution of the angle between the K_L direction and the line joining the ϕ-vertex and the K_L-vertex for $5 < r < 15$ cm, $25 < r < 35$ cm, $r > 45$ cm.

and the transverse vertex resolution, $\delta r_\perp = 0.56$ cm. The K_L vertex was accepted if

$$\delta < 4 \left[{\sigma_\delta}^2 + \left(\frac{\delta r_\perp}{d} \right)^2 \right]^{1/2}$$

If more than one K_L vertex were found (only in 0.15% of the events) we selected the vertex with the smaller angle. This cut selected 134997 events.

Different decays show different behaviour in terms of the missing momentum and the associated missing mass computed assuming the pion mass for all charged particles. Fig.5 shows the correlation of p_{mis} and M^2_{mis}: $K_L \to \pi^+\pi^-\pi^o$ decays populate the region of $M^2_{mis} = m^2_{\pi^o}$; $K_L \to \pi\ell\nu$ decays are clearly separated in two bands with $M^2_{mis} < 0$; $K_L \to \pi^+\pi^-$ decays are peaked around $p_{mis} = 0$, $M^2_{mis} = 0$; $K_L \to K_S \to \pi^+\pi^-$ "elastic" events are expected to populate the band with $p_{mis} = (-M^2_{mis})^{1/2}$.

Fig.6 shows the distribution of the K_L decay length. Fitting the distribution with an exponential in the region 40 cm $< r <$ 150 cm, we obtain $\lambda = 333 \pm 13$ cm for the average K_L decay length in good agreement with the expected value of 343

cm, thus indicating a reconstruction efficiency constant over the range of the fit.

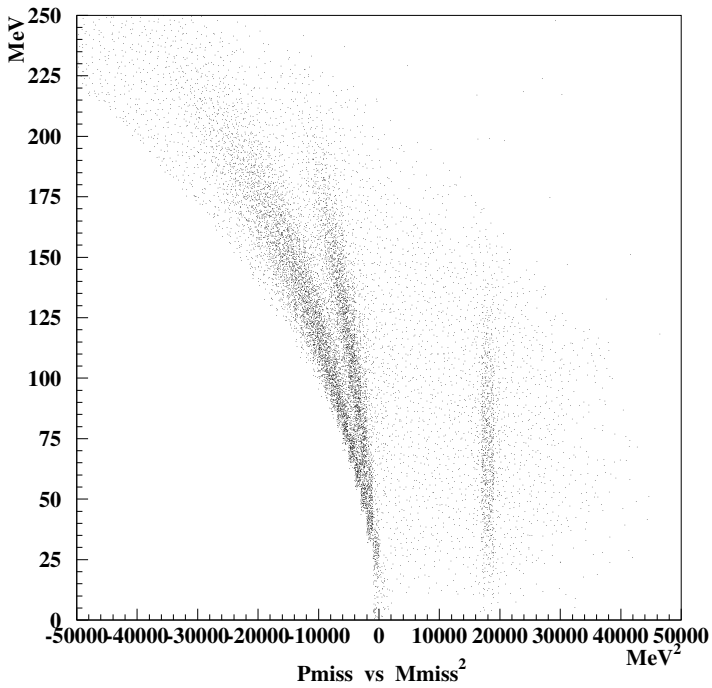

Figure 5: Correlation between the missing momentum and the squared missing mass for charged decays of the K_L

To select $K_L \to \pi^+\pi^-$ decays and $K_L \to K_S \to \pi^+\pi^-$ elastic events we required the invariant mass associated with the K_L vertex to be the neutral kaon mass. Fig.7 shows the invariant mass distribution fitted with a polynomial and a gaussian of r.m.s. width $\sigma_m = 1.1$ MeV. The distribution is divided in a signal band, $m = 497.7 \pm 4$ MeV, with 1991 events and two side-bands, $m = 491.7 \pm 2$ MeV and $m = 503.7 \pm 2$ MeV with a total of 1534 events populated mostly by K_L semileptonic decays.

The distribution of the decay distance is shown in Fig.8 for the signal band and the side-bands: the two peaks around $r = 10$ cm and $r = 28$ cm are interpreted as due to $K_L \to K_S$ regeneration in the spherical beam pipe and in the cylindrical drift chamber inner wall.

For both $K_L \to \pi^+\pi^-$ decays and $K_L \to K_S \to \pi^+\pi^-$ elastic events the absolute values of the K_S and K_L momenta should be equal. Fig.9 shows the distribution of the difference $\Delta|\vec{p}| = |\vec{p}_S| - |\vec{p}_L|$ for the signal band and the side-bands. The signal band was fitted with a gaussian centred at $\Delta|\vec{p}| = 0$ MeV with $\sigma = 2$ MeV, representing the decays and a second gaussian centred at $\Delta|\vec{p}| = 3$ MeV with $\sigma = 4$ MeV, probably representing elastic interactions where a small fraction of the momentum is transferred to the recoil nucleus. To further reduce the background of semileptonic decays we required $-6 < \Delta|\vec{p}| < +12$ MeV. This cut selected 915 events.

Fig.10 shows the distribution of the vertex distance, r, and of the projected vertex distance, $\rho = (x^2 + y^2)^{1/2}$, for the 915 events and for the side-bands sample.

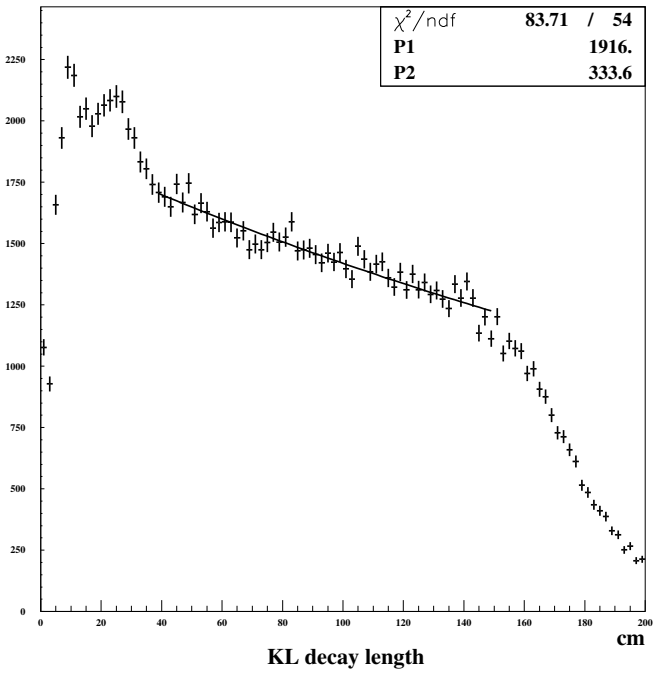

Figure 6: Distribution of the K_L decay length

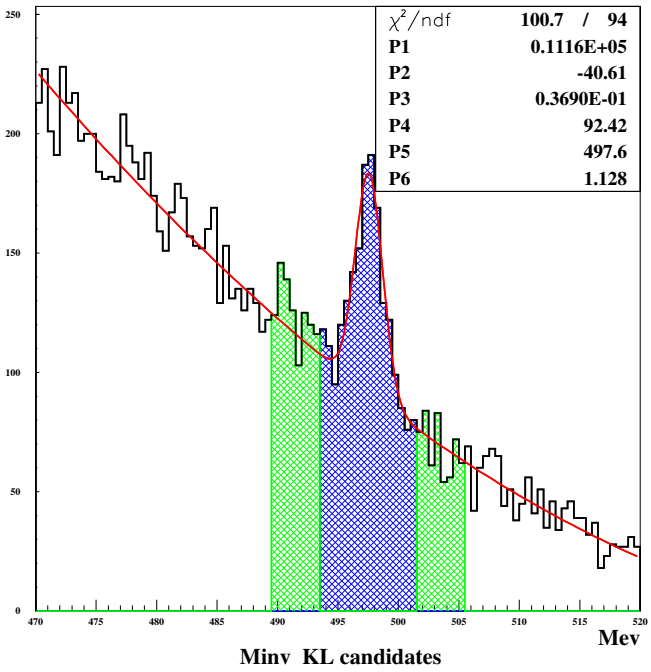

Figure 7: Distribution of the invariant mass for charged decays of the K_L

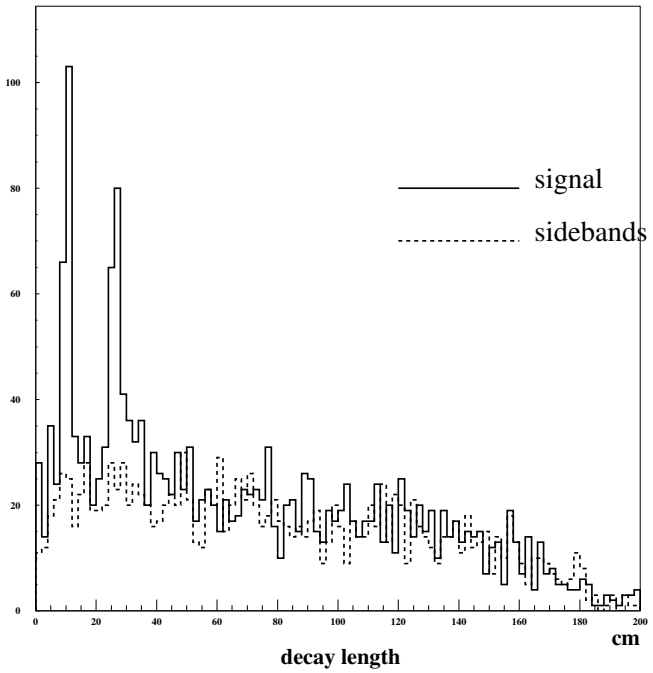

Figure 8: Distribution of the decay distance for the signal and the side bands

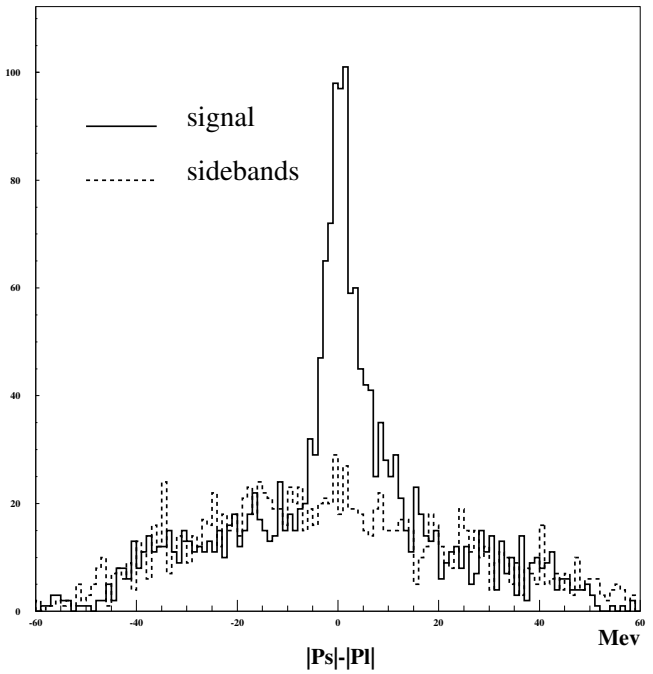

Figure 9: Distribution of the difference between the absolute values of the K_S and K_L momenta for the signal and the side bands

On the basis of the K_S decay length distribution of fig.2, two regions of interest were defined of width (-2,+4) cm around the position of the regenerators:

- the beam pipe region, 8 cm $< r <$ 14 cm, which contains 151 events
- the chamber wall region, 23 cm $< \rho <$ 29 cm, which contains 156 events.

We parametrized the r and ρ distributions of the decay vertex using two gaussians for the peaks and a linear background, and we evaluated the amount of background events in the regions of interest. The number of $K_L \to K_S \to \pi^+\pi^-$ regenerated events is then: $N_{reg}^{bp} = 123 \pm 13$, $N_{reg}^{cw} = 122 \pm 12$.

The distribution of the angle, ω, between the K_S and K_L momentum, shown in Fig.11, was used to separate the $K_L \to \pi^+\pi^-$ decays, peaked at small angles, from the K_L semileptonic decays and $K_L \to K_S \to \pi^+\pi^-$ elastic events. A cut at $\omega < 75$ mrad selected a sample of 279 $K_L \to \pi^+\pi^-$ decays.

4.2 Results

The number of $K_L \to K_S \to \pi^+\pi^-$ regenerated events is related to the regeneration cross section on nuclei, σ_{reg}, by

$$N_{reg} = N_L \; \varepsilon \; B_{S\pi\pi} \; \sigma_{reg} \; n \; t \tag{3}$$

with $N_L = N_{SL} \; e^{-r/\lambda}$ the number of K_L mesons reaching the regenerator, ε the detection efficiency, $B_{S\pi\pi}$ the $K_S \to \pi^+\pi^-$ branching fraction, n the number of nuclei of the regenerator per unit volume, t the thickness of the regenerator.

The spherical beam pipe, of radius 10 cm, is made of AlBeMet, an alloy of 61%, in volume, of Beryllium ($\rho = 1.85$ g cm^{-3}) and 39% of Aluminum ($\rho = 2.7$ g cm^{-3}) and has a thickness of 0.50 mm:

$$(nt)^{bp} = 4.93 \; 10^{21} \; cm^{-2}$$

The cylindrical drift chamber wall is made of Carbon 0.75 mm thick, 60%-fiber ($\rho = 1.72$ g cm^{-3}) and 40%-epoxy ($\rho = 1.25$ g cm^{-3}) and has a 0.20 mm thick Aluminum shield:

$$(nt)^{cw} = 6.97 \; 10^{21} \; cm^{-2}$$

The crossing angle, computed event by event, gives an average increase of the thickness of 3% for the beam pipe and of 15.5% for the chamber wall.

The detection efficiency for $K_L \to K_S \to \pi^+\pi^-$ regenerated events is the same as for $K_L \to \pi^+\pi^-$ decays selected in the analysis, the only difference being the final ω cut. The efficiency is derived from the distribution of the $K_L \to \pi^+\pi^-$ events $dN_{L\pi\pi}/dr$, the decay length in the laboratory λ, and the number of $K_S K_L$ events

$$\frac{N_{SL} \; B_{L\pi\pi}}{\lambda} \; e^{-r/\lambda} \; \varepsilon(r) \; = \frac{dN_{L\pi\pi}}{dr} \tag{4}$$

The experimental $dN_{L\pi\pi}/dr$ distribution for the 279 selected $K_L \to \pi^+\pi^-$ decays is shown in fig.12, where also the linear fit used to extract the results is shown. The region below 4 cm, coinciding with the K_S fiducial volume, has been excluded from

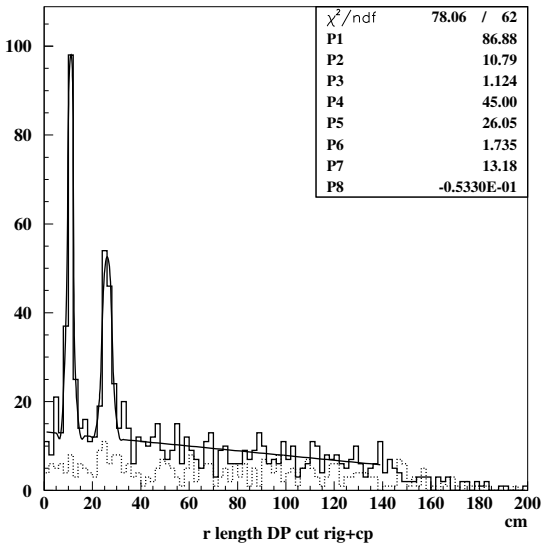

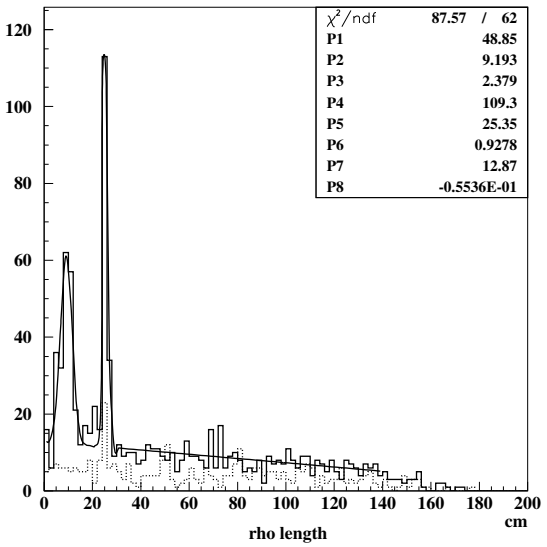

Figure 10: Distribution of the decay distance in space and of its projection on the x-y plane for $K_L \to \pi\pi$ decays and regenerated events, and for the side bands sample

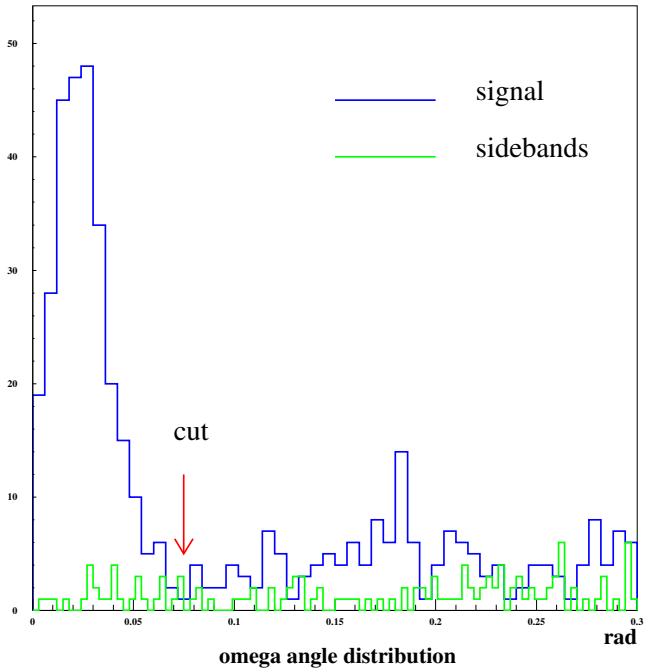

Figure 11: Distribution of the angle between the K_S and K_L momenta for the signal and the side bands

the fit to avoid ambiguities, while the region above 140 cm has a drop in efficiency, being near the edge of the drift chamber volume.

From the relations 3 and 4 we obtain

$$\sigma_{reg} = \frac{B_{L\pi\pi}}{B_{S\pi\pi}} \frac{1}{\lambda\, dN_L/dr} \frac{N_{reg}}{\langle nt \rangle} \tag{5}$$

$(dN_{L\pi\pi}/dr)$ was evaluated at the average radius of each region of interest, yielding: $(dN_{L\pi\pi}/dr)^{bp} = 2.65 \pm 0.19\ cm^{-1}$, $(dN_{L\pi\pi}/dr)^{cw} = 2.41 \pm 0.15\ cm^{-1}$. We obtain

$$\sigma_{reg}^{Be-Al} = (75.7 \pm 9.6\ _{stat})\ mb$$

$$\sigma_{reg}^{C-Al} = (51.9 \pm 6.2\ _{stat})\ mb$$

where both the statistical errors coming from the event counting and the efficiency evaluation have been included.

The angular distribution for regenerated events in the beam pipe and in the chamber wall is shown in Fig.13. To reduce the background only events in 10 cm $< r <$ 13 cm, for the beam pipe, and in 24 cm $< \rho <$ 27 cm, for the drift chamber wall were used. The small contamination from $K_L \to \pi^+\pi^-$ events is fully contained in the first bin, as was checked in the selected $K_L \to \pi^+\pi^-$ sample. The background from semileptonic decays is negligible, according to montecarlo estimations.

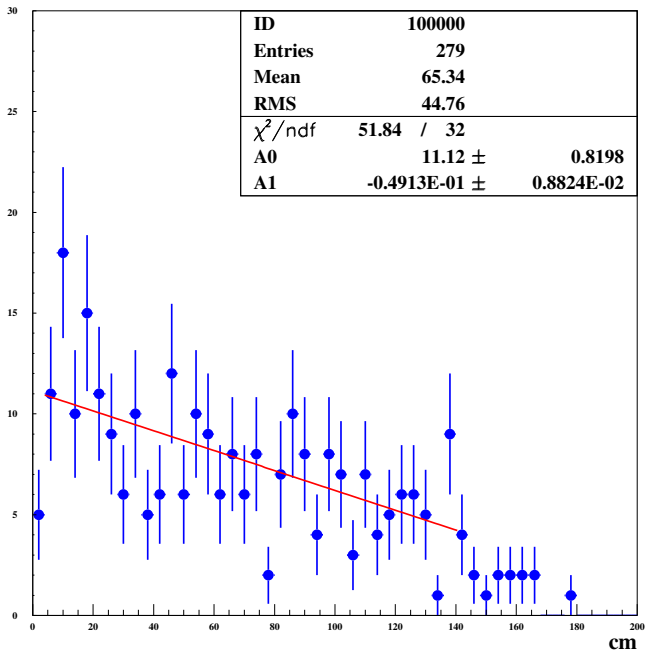

Figure 12: Radial distribution of the CP violating $K_L \to \pi^+\pi^-$ decays, selected from data as explained in the text

4.3 Systematic error

Three main categories of systematic error sources have been considered:

- event counting method;
- efficiency evaluation;
- regenerator thickness.

For the first category two sources of error have been studied: the definition of the regions of interest (r.o.i) and the shape of the fit to the background. The r.o.i. limits were varied of $\pm$ 1 cm obtaining maximum variations of about 3% for the beam pipe events and of 2% for the drift chamber wall events. Various polynomial shapes were also fitted to the background, obtaining $2 \div 3\%$ variations on the beam pipe events, but much smaller (less than 1%) on the drift chamber wall.

The efficiency evaluation is based on the assumption that regenerated K_S charged decays are detected with the same efficiency as the CP violating $K_L \to \pi^+\pi^-$ decays. A montecarlo study of such assumption [10] shows that differences in efficiency can be expected up to 2%.

A possible contamination of regenerated K_S decays in the $K_L \to \pi^+\pi^-$ sample could bias the measurement to higher efficiencies. To account for this effect the $K_L \to \pi^+\pi^-$ radial distribution, showed in fig.12, was fitted adding to the main linear shape two gaussians centered at the regenerators positions (just as was done in

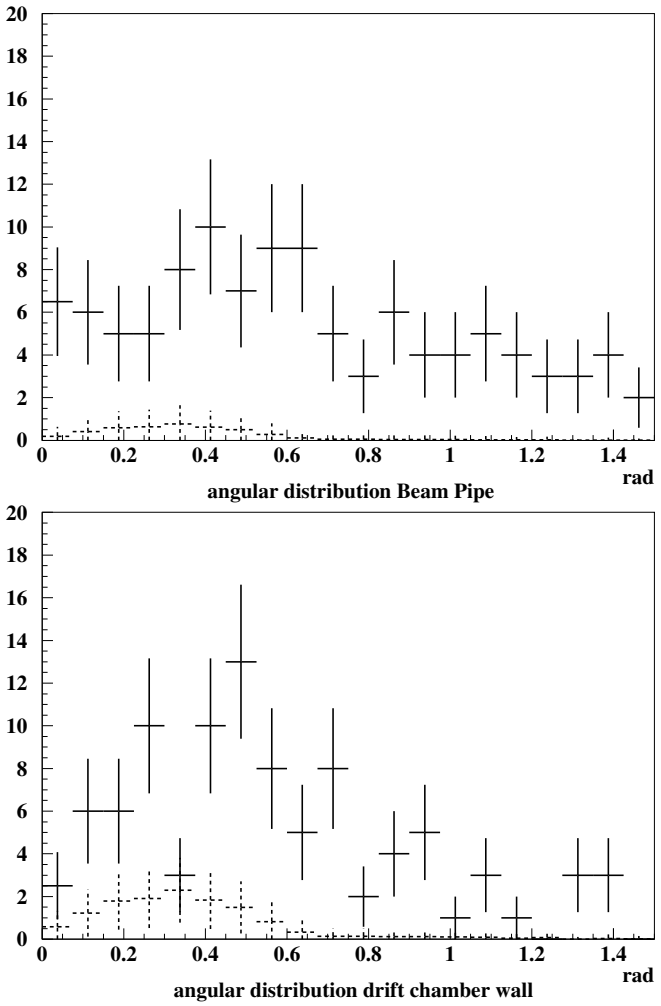

Figure 13: Angular distribution of $K_L \to K_S$ regenerated events in the beam pipe and in the drift chamber wall

fig.10). The data are compatible with absence of contamination on the drift chamber wall, but (probably due to a statistical fluctuation) allow a non negligible contamination on the beam pipe, which results in a considerably reduced efficiency (7÷8%). This turns out to be the main systematic error (non related to the regenerators knowledge) on this measurement.

Finally the beam pipe thickness is known with a precision of $50\,\mu m$, according with the production tolerances. For the drift chamber wall an uncertainty of $\pm 50\,\mu m$ on both carbon and aluminum was estimated from the study of the multiple scattering of e^+e^- pairs.

The systematic error sources are summarized in table 3.

error source	$\Delta\sigma^{Be-Al}\,(mb)$	$\Delta\sigma^{C-Al}\,(mb)$
r.o.i. limits	2.5	1.0
backgr. shape	2.0	0.4
$\varepsilon_{cp} \neq \varepsilon_{reg}$	1.5	1.1
regen. contam. in $K_L \to \pi^+\pi^-$	6.5	3.7
regenerators thickness	7.6	3.5
total	10.6	5.3

Table 3: Systematic error contributions.

5 Conclusions and discussion

On the basis of the first data collected during the commissioning of DAΦNE the KLOe experiment has analyzed $\sim 1.4\,10^5$ $\phi \to K_L K_S$ decays with both kaons decaying to charged particles. Using Bhabha scattering events to precisely define the collision region, and fitting the distribution of the $K_S \to \pi^+\pi^-$ decay vertex, the K_S decay length is measured as:

$$\lambda_s \;=\; 5.78 \;\pm\; 0.08\,(stat) \;\pm\; 0.10\,(syst)\,mm.$$

The average K_L decay lenght is $\lambda_L = 333 \pm 13\,(stat)$ cm. A sample of 279 $K_L \to \pi^+\pi^-$ CP-violating decays is clearly identified with negligible background, and is used to measure the efficiency for reconstructing $K_L \to K_S \to \pi^+\pi^-$ events due to regeneration in the beam pipe and in the drift chamber inner wall.

The cross section in the beam pipe made of a 61%Beryllium-39%Aluminun alloy is

$$\sigma^{Be-Al} = 75.7 \pm 9.6_{stat} \pm 10.6_{syst}\,mb$$

The regeneration cross section in the drift chamber wall made mainly of Carbon is

$$\sigma^{C-Al} = 51.9 \pm 6.2_{stat} \pm 5.3_{syst}\,mb$$

With this data it is not possible to evaluate separately the regeneration cross section on Beryllium, Carbon and Aluminun nuclei unless we make additional hypotheses on its dependence upon the atomic mass. Theoretical calculations [8] based on the eikonal approximation are shown in Fig.14 as well as a measurement on Beryllium

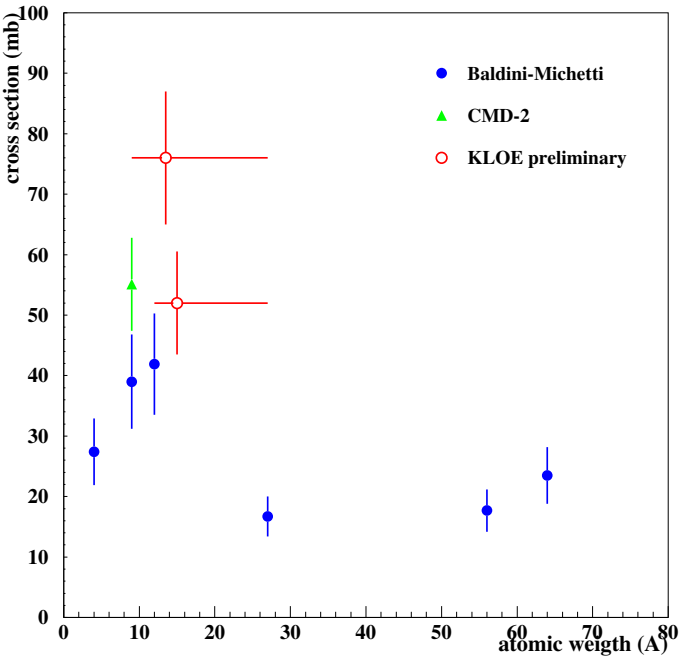

Figure 14: $K_L \to K_S$ regeneration cross section as a function of the atomic mass.

ref.[11] [12] made with the CDM-2 detector at the Novosibirsk VEPP-2M electron-positron collider. The theoretical predictions do not show any evident dependence upon the atomic mass due to the interference of the K and $\bar{K}$ amplitudes that have different behaviour as a function of A. However our measurements can hardly accomodate a cross section on Alluminium nuclei smaller than for Beryllium and Carbon, as shown in fig.15 where the correlation between the values of the cross sections is drawn.

References

[1] S.Guiducci et al., *DAΦNE Operating Experience*, Proceedings of PAC99, New York, March 1999.

[2] S.Bertolucci, *A Status Report of KLOE at DAΦNE*, Proceedings of the 19th International Conference on Lepton and Photon Interactions at High Energy, Stanford 1999.

[3] C.Bloise,M.Incagli,*The event classification module and the ECLO, ECLS banks*, KLOE memo 175, 1/99.

[4] *Status of the KLOE Detector*, Proc. of DAΦNE99, Frascati (1999).

[5] S.Dell'Agnello,*TRKMON, The Tracking Monitor Program of KLOE*, KLOE Memo 202, 1/99.

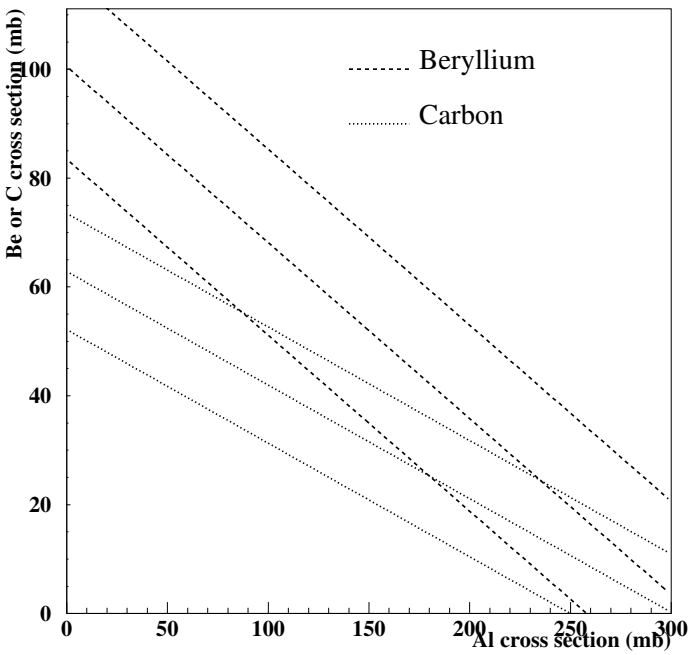

Figure 15: Beryllium and Carbon cross section as a function of the Alluminum regeneration cross section.

[6] A.Pais and O.Piccioni, Physical Review 100 (1955) 1487

[7] K.Kleinknecht, Fortschritte für Physik 21 (1973) 57

[8] R.Baldini and A.Michetti, *K_L interactions and K_S regeneration in KLOE*, LNF-96-008 (IR), 16.2.1996.

[9] M.Palutan, *CP-violation study at DAΦNE: the trigger of the KLOE experiment*, Ph.D. Thesis, University of Rome "Tor Vergata", 1999.

[10] A.Ferrari, *Measurement of the $K_L \to K_S$ regeneration cross section in the KLOe experiment at DAΦNE*, Ph.D. Thesis, University of Rome "La Sapienza", 1998.

[11] E.P.Solodov, *Study of the rare K_S, K_L, K^+, K^- decays at the ϕ resonance with the CMD-2 detector*, Proceedings of the 29th International Conference on High Energy Physics, A.Astbury, D.Axen and J.Robinson eds., World Scientific 1999, p.1046.

[12] E.P.Solodov, *Studies of kaon decays at the ϕ resonance*, Proceedings of the 1999 Workshop on Kaon Physics, eds. J.L.Rosner and B.R. Winstein, The University of Chicago Press, p.311.